Journal of Physics D: Applied Physics

PAPER

Compact multi-resonator ventilated duct silencer with broadband sound attenuation and steady airflow

Joshua Lloyd, Chadi Ellouzi, Farhood Aghdasi and Chen Shen*

Department of Mechanical Engineering, Rowan University, Glassboro, NJ 08028, United States of America
* Author to whom any correspondence should be addressed.

E-mail: shenc@rowan.edu

Keywords: reactive silencer, duct acoustics, sound attenuation, acoustic metamaterial, flow resistance

OPEN ACCESS

RECEIVED
2 October 2025

REVISED
7 December 2025

ACCEPTED FOR PUBLICATION
15 December 2025

PUBLISHED
29 December 2025

Abstract

This research presents the design of a compact acoustic metamaterial duct silencer capable of attenuating a wide range of frequencies while allowing steady airflow. The proposed device incorporates a series of space-folded slit resonators, each exhibiting a different length tailored to attenuate a specific frequency. Combining these side-loaded resonators onto a host tube achieves broadband noise reduction thanks to the cumulative effects of the individual components and their synergistic interactions. Compared with many traditional duct silencers and mufflers, this design enables unobstructed flow through its central region, resulting in a much lower fluid pressure drop across the structure. Additionally, the use of space-folded resonators results in a significant reduction in the overall diameter of the device, leading to a high efficiency of volume usage. Theoretical calculations based on the transfer matrix method and numerical simulations using finite element analysis are used to validate the structure. Implementing a geometry generation function allows the structure to be parametrically optimized to suppress noise within given frequency ranges. Using these methods, a design is carried out that maximizes transmission loss (TL) from 650 Hz to 2000 Hz with the outer diameter of the structure constrained to 0.2 m. The cumulative effect of the tuned resonator slits results in an average measured TL of 36.3 dB within the target frequency range in the stationary scenario and 17.2 dB under grazing flow. The demonstrated utility of the silencer in achieving comprehensive noise control while maintaining low flow resistance makes it a promising candidate for various applications such as automotive exhaust systems, industrial machinery, and naval vessels. Our demonstration paves the way for the development of new duct silencers that can meet the growing demand for effective noise control in various settings where unrestricted fluid flow and broadband attenuation are paramount.

1. Introduction

Broadband noise reduction is crucial for controlling sound propagation in ducts, such as automotive mufflers, industrial pipelines, and HVAC systems. Because of the tight spaces in which ducts are typically located, the design of duct silencers is usually accompanied with stringent size and geometric requirements. Another important consideration is the bandwidth as broadband sound attenuation is always desired to maximize the effectiveness of noise mitigation. In addition to this, special considerations for low-frequency noise must be made, which represents a challenging task due to the weak dissipative ability of most materials [1]. Finally, flow resistance of the duct silencer is an important property in systems requiring unrestricted fluid flow. Many noise control techniques used in open-room acoustics are not suitable for applications involving ducted flow due to the obstructions that would be placed within the path of the fluid.

One common approach to passive airborne sound reduction is through absorption of the incident wave energy. Conventional sound absorbers are typically in the form of porous materials [2]. These absorbative materials dissipate acoustic energy through thermo-viscous interactions within the viscous

boundary layer of their surfaces [3]. A major disadvantage of porous media absorbers is the difficulty in low frequency sound absorption. While high-frequency energy can easily be reduced by viscous dampening inside a thin layer of material, lower-frequencies require the thickness of the material to be significantly larger to have any effect [4]. To overcome this limitation, complex structures with embedded porous materials have been proposed which enhance their acoustic performance [5–9]. In a different approach, metamaterial acoustic black holes (ABHs) have recently become a study of interest to achieve quasi-perfect sound absorption without the use of porous materials [10, 11]. Though broadband attenuation can be achieved with this method, the flow is significantly impeded within the duct due to the structure. Bravo and Maury [12] proposed an ABH metamaterial structure that achieves broadband noise absorption without obstructing the path of fluid flow through the duct. Experimental results showed a transmission loss (TL) of 25–40 dB from 1400–1900 Hz.

Alternatively, reactive silencers use reflection rather than absorption as the primary mechanism to achieve sound attenuation. Reactive silencers function by inducing a large impedance mismatch in the structure which causes the incident sound wave to be reflected backwards. Classical examples of reactive silencers include Helmholtz resonators, quarter-wave resonators (QWRs), and expansion chambers [13]. Helmholtz resonators and QWRs in duct acoustics are typically side-branch resonators (SBRs) which are side-loaded to the main duct allowing for the free-movement of fluid through the duct [14, 15]. These structures have a narrow attenuation peak, resulting in strong impedance mismatch in only a tight frequency range [16, 17]. To overcome this limitation, acoustic metamaterials which contain complex structures consisting of multiple SBRs have become a topic of large interest in recent years. Structures with periodic arrays of Helmholtz resonators [18–21], mechanically coupled Helmholtz resonators [22], and periodic arrays of tube resonators [23] have been explored to this end. Silencers containing space-folded Helmholtz resonators have also been explored to increase radial compactness while achieving significant attenuation [24]. Červenka *et al* [25] studied the effects of rectangular QWRs side-loaded to a duct of rectangular cross-section. Using 6 detuned resonators, the optimized structure achieves good TL in a relatively narrow band from 250 Hz to 350 Hz. The authors found that dissipation through viscothermal losses in the structure only slightly improves the overall TL and that optimization of absorption does not lead to an optimal TL. It was also discovered that the minimum TL increases linearly with the number of resonators for a given frequency range. In a continuation of this research, Červenka and Bednařík [26] proposed an axisymmetric cylindrical design similar to their previous study. This structure consists of an array of SBRs in the form of thin cylindrical disks. Using optimization techniques to calculate the geometric dimensions of the disks, the authors presented a design with minimum TL of 28.9 dB from 100–700 Hz. This geometry shows promise for low-frequency attenuation but has a practical limitation of radial size.

In recent years, advancements in complex acoustic metamaterials have targeted the design of noise control systems that simultaneously address passive ventilation requirements [27–29]. These metamaterials generally consist of sub-wavelength unit cells with a highly open structure, allowing for airflow while achieving acoustic control otherwise unattainable with conventional structures. Numerous duct-integrated structures have been developed in the context of mufflers and silencers, such as expansion chambers with integrated acoustic metamaterial baffles (AMBs) [30, 31], acoustic insulation vented channels [32], space-folded metamaterial mufflers [33], virtual Herschel–Quincke tube systems [34], Fano-like interference based mechanisms [35, 36], and unit cells for duct and pipeline coatings [37, 38]. In addition to duct-based metamaterials, structures have been proposed to address acoustic attenuation for other ventilated systems in free space such as in windows or large vents [39–42], especially at low frequencies [43, 44]. These structures can be configured in an array fashion to effectively cover extensive surface areas leading to a wide range of applications. Many origami-based acoustic metamaterials have also been developed, incorporating complex folding patterns to achieve sound suppression while maintaining high flow permeability [45, 46]. Lastly, AMBs such as the locally resonant acoustic metamaterials exhibit promising results to improve existing silencer designs [47]. Nevertheless, the impact of flow resistance is evaluated independently in most studies [27, 29, 48], and the acoustic performance under actual flow conditions has yet to be validated. Moreover, many existing structures exhibit irregular or complex shapes, making them difficult to be applied to well-defined or confined spaces.

This research proposes a broadband, compact metamaterial reactive duct silencer which addresses many of the limitations and restrictions associated with duct silencers requiring high flow efficiency. For example, common designs face challenges including a lack of necessary radial compactness required for widespread implementation, limited custom adaptability to individualistic needs, reduced flow efficiency due to obstructions in the flow path, and relatively narrowband attenuation. Such issues are addressed in this work through the development of a novel geometric layout which allows for a high degree of radial compactness while maintaining highly tunable broadband capabilities without obstructing flow

paths. The silencer consists of multiple arrays of space-folded concentric resonating 'slits' arranged in discrete sections positioned axially along the waveguide. Each resonator slit has a unique length and is detuned in relation to all other resonators. This yields a large effective frequency range as each resonator is designed to operate at a specific frequency. The resultant space-folded design greatly increases radial compactness with only a small reduction in axial compactness. In addition, the use of side-branch reactive resonators ensures that the main duct is free from obstructions, leading to efficient fluid-flow with minimal pressure drop. Theoretical calculations and numerical simulations are performed to validate the effectiveness of the structure. Experimental measurements are also carried out both with and without background flow conditions, showcasing an average TL of 36.3 and 17.2 dB, respectively within the target frequency band. The results confirm the practical utility of the silencer when airflow is present. Our work demonstrates an efficient and versatile approach for the design of duct silencers and could serve as a viable solution for noise control applications where high ventilation and broadband performance are required.

The remaining sections are arranged as follows. Section 2 explains the structure's design and presents an analytical model for the muffler using the transfer matrix method (TMM). In addition, a bend correction factor is derived to account for the folded geometry of the slit resonators. The theoretical calculation is then validated using a finite element method (FEM) in section 3 through a set of parametric studies. The final optimized muffler is also detailed. Section 4 presents the experimental results of the optimized muffler in both stationary and grazing flow conditions. Finally, the conclusions of this research are given in section 5, including remarks on possible future improvements.

2. Design and analytical modeling

2.1. Geometry design

The design concept of the proposed structure is illustrated in figure 1. The basic structure contains a main duct and an array of side-loaded cylindrical resonator slits with an axially decreasing radial length. Cambonie *et al* [49] have shown that a cylindrical QWR is able to be bent while maintaining the original properties of the unbent resonator. While a small frequency shift is observed, it is within a reasonable range and can be accounted for during the design. As Červenka and Bednařík have shown [25, 26], annular cavities behave similarly to QWRs such that each resonator's radial length corresponds to the resonance frequency of that resonator. Thus, the proposed resonator slits can be rearranged and bent in such a way to fully occupy the space around the main duct, allowing for a smooth and planar outer surface profile. The final muffler consists of N_c number of discrete axial sections, denoted here as 'cells', each containing N_r number of individual resonators. Figure 2 shows the proposed design along with a cross-sectional view of a single axisymmetric cell. The main duct has a circular cross-section with radius R_d and contains $i = 1, \ldots, N_c N_r$ resonators where $N_c, N_r > 0$. $R_{cav,i}$ describes the equivalent radial length of the ith resonator slit in its un-folded state and is measured along the neutral line of the bent cavity. The wall thickness and axial entrance length of the resonator cavities are assumed to be fixed for the structure and are defined as d_t and L_{cav}, respectively. The total cross-sectional width and height of the nth cell are given by W_n and H, respectively.

While it is intuitive to arrive at the final dimensions of the muffler by forming the structure as described above and in figure 1, an alternate method of describing the muffler is used which simplifies dimensional calculations. Considering that, to obtain broadband attenuation, the structure should be designed such that $R_{cav,i}$ is periodically varied as the axial dimension z increases, it is evident that each cell must also have an axially varying W_n. By introducing a width scaling factor, SF_w, W_n is now described by $W_n = W_1 + (n-1)\,SF_w$ where W_1 is the initial cell width.

$L_{w,i}$ is an important variable which defines the axial length of the wall separating the i and $i+1$ resonators. When i is not equal to N_r,we have $L_{w,i} = d_t$. However, due to the folded nature of the structure, it is observed that the length of wall separating the final resonator of the n and $n+1$ cells is larger than d_t. Therefore, when i is equal to N_r, $L_{w,i}$ spans the distance between n and $n+1$ cells. $L_{w,i}$ is mathematically described as follows:

$$L_{w,i} = \begin{cases} d_t, & i \neq N_r \\ W_n - (N_r L_{cav} + (N_r - 1)\, d_t), & i = N_r \end{cases}. \tag{1}$$

It is noted that, as implemented later in section 3, the parameter L_{cav} is solved along with $L_{w,i}$ using a system of linear equations. This will help prevent an over-defined, unsolvable geometry in many cases since the definitions of W_n, H, N_r, and d_t are sufficient to fully define the cell geometry.

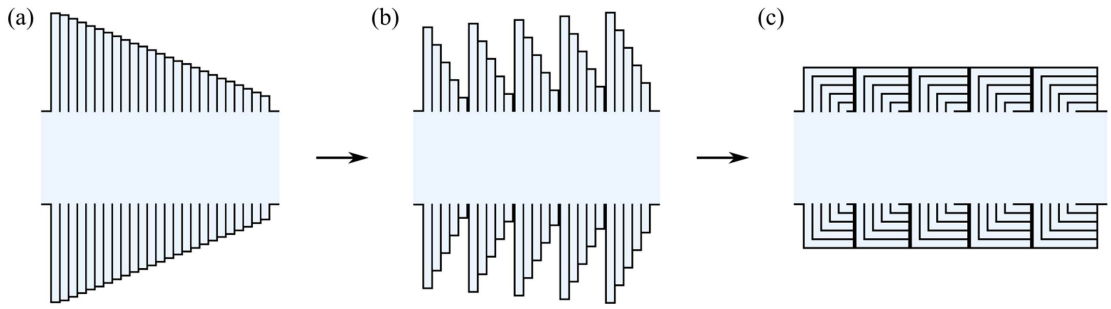

Figure 1. Design concept of the broadband duct silencer. (a) A series of unarranged unfolded slit resonators with different lengths can achieve broadband sound attenuation. (b) Arranging the slit resonators helps to achieve a more uniform geometric profile. (c) The slit resonators are further folded to best utilize the space, which results in a compact structure with planar surface profiles.

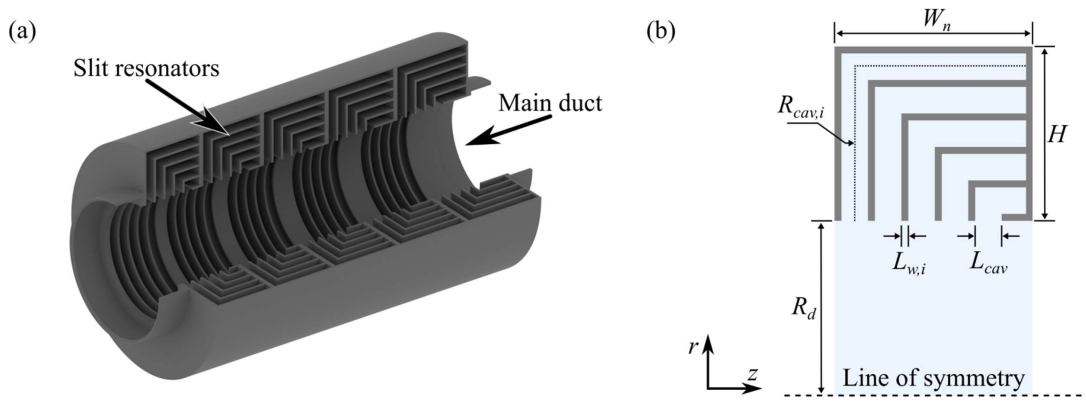

Figure 2. (a) Sectional cutaway of design, (b) cross-section of a single axisymmetric cell.

2.2. TMM

The TMM is a widely used method for analyzing the performance of acoustic structures as it allows for complex systems to be broken into simpler components [50]. The representative matrices of these components are then multiplied together, yielding an overall transfer matrix which can be used to directly calculate the necessary performance characteristics. To evaluate the analytical performance of the muffler, the resonator cavities are first resolved with an acoustic admittance relative to the main duct. The duct walls are assumed to be sound-hard barriers, and the duct length is assumed to be infinite to eliminate reflections at the ends.

We start by defining the low-frequency wall admittance of the ith resonator slit, ignoring visco-thermal interactions, which is expressed as [12]:

$$y_i = -j\frac{J_1(k_0R_\mathrm{d})H_1[k_0(R_\mathrm{d}+R_{\mathrm{cav},i})] - J_1[k_0(R_\mathrm{d}+R_{\mathrm{cav},i})]H_1(k_0R_\mathrm{d})}{J_0(k_0R_\mathrm{d})H_1[k_0(R_\mathrm{d}+R_{\mathrm{cav},i})] - J_1[k_0(R_\mathrm{d}+R_{\mathrm{cav},i})]H_0(k_0R_\mathrm{d})} \tag{2}$$

where k_0 is the acoustic wavenumber. J_0, J_1 are the Bessel functions of the first kind with order 0 and 1, respectively, and H_0, H_1 are the Hankel functions of the first kind with order 0 and 1, respectively. Following this, the ith resonator volume admittance can be expressed as:

$$Y_i = \frac{2\pi R_\mathrm{d}L_\mathrm{cav}y_i}{Z_0} \tag{3}$$

where $2\pi R_\mathrm{d}L_\mathrm{cav}$ defines the resonator entrance area. Here, the background medium is air and its characteristic impedance is $Z_0 = \rho_0 c_0$ where ρ_0 is the density and c_0 is the speed of sound. With the volume admittance for the ith resonator now obtained, the TMM can be used to evaluate the full structure. The general expression for the TMM is given by:

$$\begin{bmatrix} p \\ v \end{bmatrix}_{z=0} = \begin{bmatrix} M_{11} & M_{12} \\ M_{21} & M_{22} \end{bmatrix} \begin{bmatrix} p \\ v \end{bmatrix}_{z=L_\mathrm{tot}} \tag{4}$$

where L_{tot} is the total length of the fluid. The pressure p and velocity v of the incident wave at the structure's inlet are related to those at the outlet by a transfer matrix $\boldsymbol{M}$. Continuing with this formulation, the matrices representing the fluid layer in the main duct are:

$$\boldsymbol{M}_1 = \begin{bmatrix} \cos(k_0 L_{\text{cav}}) & j\frac{Z_0}{S}\sin(k_0 L_{\text{cav}}) \\ j\frac{S}{Z_0}\sin(k_0 L_{\text{cav}}) & \cos(k_0 L_{\text{cav}}) \end{bmatrix} \tag{5}$$

$$\boldsymbol{M}_{2,i} = \begin{bmatrix} \cos(k_0 L_{\text{w},i}) & j\frac{Z_0}{S}\sin(k_0 L_{\text{w},i}) \\ j\frac{S}{Z_0}\sin(k_0 L_{\text{w},i}) & \cos(k_0 L_{\text{w},i}) \end{bmatrix}. \tag{6}$$

Here, $\boldsymbol{M}_1$ represents the fluid layer spanning the width of the resonator entrance, L_{cav}, within the main duct, while $\boldsymbol{M}_{2,i}$ accounts for the fluid layer spanning the wall, $L_{\text{w},i}$, separating i and $i+1$ resonators in the duct. S denotes the cross-sectional area of the duct. The third matrix necessary for resolving the full characteristics of the structure is given by:

$$\boldsymbol{M}_{3,i} = \begin{bmatrix} 1 & 0 \\ Y_i & 1 \end{bmatrix} \tag{7}$$

$\boldsymbol{M}_{3,i}$ resolves the ith SBR slit using the volume admittance Y_i given by equation (3). With the individual transfer matrices obtained, the overall transfer matrix can be calculated by multiplying the individual transfer matrices together for all $i = 1, \ldots, N_{\text{c}}N_{\text{r}}$:

$$\boldsymbol{M} = \prod_{i=1}^{N_{\text{c}}N_{\text{r}}} \boldsymbol{M}_1 \boldsymbol{M}_{2,i} \boldsymbol{M}_{3,i} = \begin{bmatrix} M_{11} & M_{12} \\ M_{21} & M_{22} \end{bmatrix}. \tag{8}$$

The final transmission coefficient is obtained as:

$$\tau = \left| \frac{2\mathrm{e}^{jk_0 L_{\text{tot}}}}{M_{11} + \frac{S}{Z_0}M_{12} + \frac{Z_0}{S}M_{21} + M_{22}} \right|^2. \tag{9}$$

This analytical model provides an efficient way to estimate the performance of the structure and is used for parametric optimization during the design as it allows for rapid computation for various geometries.

2.3. Viscothermal model

Losses due to viscothermal interactions within the structure are accounted for using an equivalent fluid model. Originally put forth by Zwikker and Kosten [51] and later analyzed in tubes of various cross section by Stinson [52], the model simplifies the Kirchhoff sound propagation theory with considerable accuracy. Following this approach, here an equivalent complex density ρ_{eff} and sound speed c_{eff} are assigned to the resonator slits [25, 26], namely:

$$\begin{cases} \rho_{\text{eff}} = \frac{\rho_0}{\Psi_v} \\ c_{\text{eff}} = c_0 \sqrt{\frac{\Psi_v}{\gamma - (\gamma-1)\Psi_h}} \end{cases} \tag{10}$$

with

$$\Psi_a = 1 - \frac{\tanh\left(\frac{\lambda_a L_{\text{cav}}}{2}\right)}{\frac{\lambda_a L_{\text{cav}}}{2}}, \quad a = v, h \tag{11}$$

and

$$\begin{cases} \lambda_v = \sqrt{\frac{j\omega\rho_0}{\mu}} \\ \lambda_h = \sqrt{\frac{j\omega\rho c_p}{\kappa}} \end{cases}. \tag{12}$$

Here, $\gamma = 1.4$ is the adiabatic constant, $\mu = 1.83 * 10^{-5}$ Pa the dynamic viscosity, $c_p = 1004\,\text{Jkg}^{-1}\text{K}^{-1}$ the specific heat, and $\kappa = 25.9 * 10^{-3}\,\text{Wm}^{-1}\text{K}^{-1}$ the coefficient of thermal conductivity. ρ_{eff} and c_{eff} are used to define a complex effective wavenumber, $k_{\text{eff}} = \omega {c_{\text{eff}}}^{-1}$, for the wall admittance of the resonator slits in equation (2). The characteristic impedance in equation (3) is also updated with a complex effective characteristic impedance $Z_{0,\text{eff}} = \rho_{\text{eff}} c_{\text{eff}}$.

Table 1. Resonance frequencies of straight f_s and bent f_b resonator slits at various resonator lengths, R_{cav}.

R_{cav} (m)	0.1094	0.0902	0.0710	0.0518	0.0326
f_s (Hz)	585	726	943	1324	2128
f_b (Hz)	645	795	1026	1425	2265

2.4. Bend correction

To best utilize the space of the silencer, all resonating slits are bent 90° to form an annular disk-shaped resonator that can fit compactly on the main tube. Similar to a cylindrical QWR whose resonance frequency can upshift due to bending [49], here we need to account for this effect by considering a small correction factor. A numerical model in COMSOL Multiphysics is employed to determine the value and order of this correction factor. The Pressure Acoustics physics model in the frequency domain is used along with a thermally conducting and viscous fluid model. A thermoviscous boundary layer impedance is added around the walls of the resonators to account for absorption due to viscous interactions, and the walls are considered rigid. The inlet and outlet of the duct are defined as ports to calculate the interaction and propagation of acoustic waves in the domain. Plane waves are strictly analyzed by setting the input port's azimuthal mode to 0, limiting input wave generation to have no angular variation. Additionally, no reflections are generated at the input and output ports, allowing for accurate analysis of the resonators' acoustic properties.

The geometry is 2D-axisymmetric along the z-axis with the radius of the main duct defined as $R_d = 0.050$ m and the total length as $L_{tot} = 0.425$ m. To determine the correction factor, a series of straight cylindrical resonators at various radial lengths are simulated, followed by a series of bent resonators of equivalent length R_{cav}. The axial length of the resonators is chosen as $L_{cav} = 0.0076$ m. The resonators are positioned at the halfway point between the inlet and outlet of the duct and are simulated one at a time. The location of the bend within the resonators is chosen to be at $0.5R_{cav}$. The simulated resonance frequencies of each resonator slit are shown in table 1.

It is seen that bending a cylindrical resonator disk results in a frequency upshift relative to the unbent resonator of equal length which corresponds to the results discussed in [49]. Using the data presented in table 1, two power-law equations can be derived which approximately relate the resonance frequencies of the straight (f_s) and bent (f_b) resonators in Hertz to the lengths R_{cav}:

$$f_s \approx 55.767 {R_{cav}}^{-1.066} \tag{13}$$

$$f_b \approx 65.539 {R_{cav}}^{-1.037}. \tag{14}$$

If it is instead assumed that f_s is equivalent to f_b, and R_{cav} in equation (13) exchanged for some effective length, say R_{eff}, then equation (13) is rewritten as:

$$f_b \approx 55.767 {R_{eff}}^{-1.066}. \tag{15}$$

Equations (14) and (15) are then equated and solved for R_{eff}, leading to the final equation:

$$R_{eff} \approx 0.86 {R_{cav}}^{0.973} \tag{16}$$

where R_{eff} is the corrected effective resonator length in meters. $R_{cav,i}$ is then replaced by $R_{eff,i}$ in equation (2). It is noted here that the choice of L_{cav} is insignificant to the bend correction upshift and can be chosen arbitrarily. In addition, the location of the bend within the space-folded resonators does exhibit an impact on the upshifted peak frequency. Nevertheless, its effect is small and is neglected here for simplicity.

3. Numerical validation and parametric optimization

3.1. Numerical validation with parametric studies

To validate the theoretical calculations of the analytical model, parametric studies are performed using the TMM model as well as a numerical FEM approach. These studies compare the TMM theory with the FEM model to assess the influence of various geometric properties on the muffler's acoustic performance.

Building on the FEM model given in section 2.4, simulations are executed up to the cutoff frequency of the first higher-order mode of the duct $f_h \approx 1.841c/(2\pi R_d) = 2011$ Hz. The waveguide is modeled

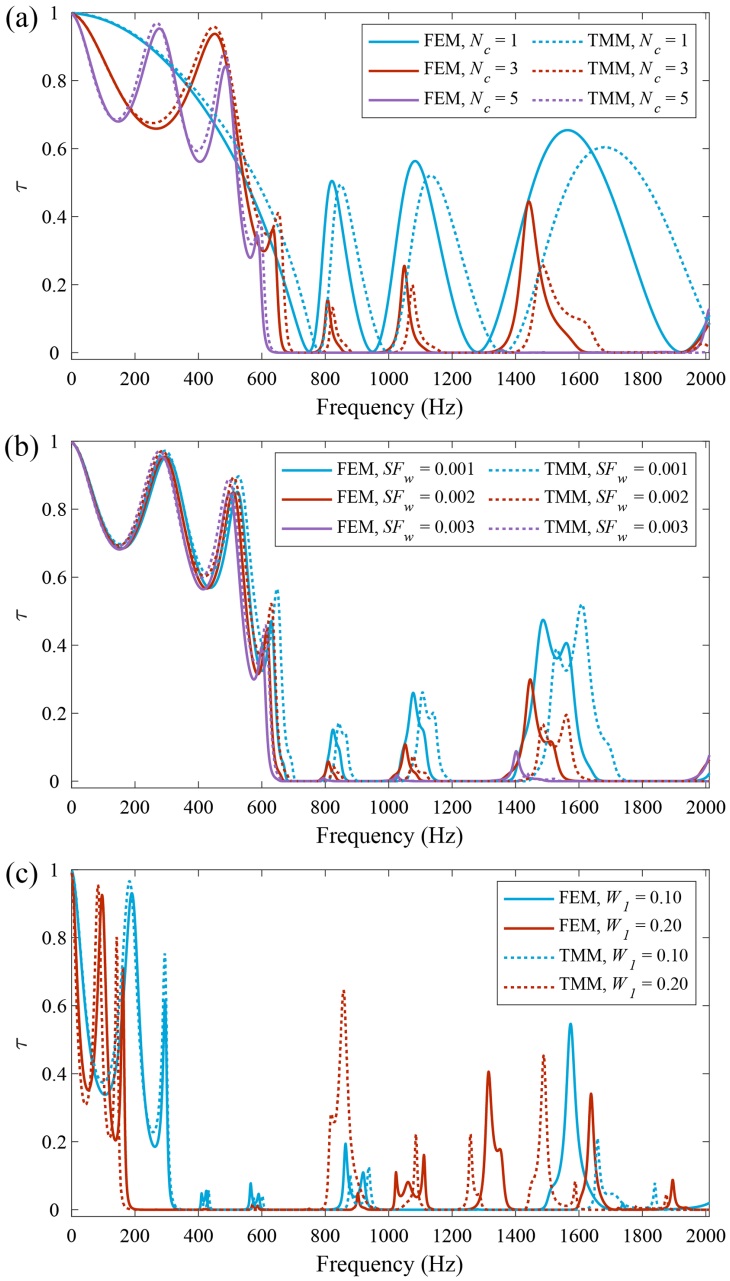

Figure 3. Comparative transmission coefficient between FEM and TMM based on different parameters. (a) Various cell numbers. (b) Various width scaling factors. (c) Various initial cell widths.

with stationary air and a sound speed $c_0 = 343.2\,\mathrm{m\,s^{-1}}$, ambient density $\rho_0 = 1.204\,\mathrm{kgm^{-3}}$, and ambient temperature $T_0 = 293.15\,\mathrm{K}$. The geometry is again simulated as 2D-axisymetric along the z-axis with $R_\mathrm{d} = 0.050$ m. In all cases, wall thickness is fixed at 0.002 m.

The first parametric study is conducted for structures with cell numbers $N_\mathrm{c} = 1$, 3, and 5 to evaluate the coupling effects among the cells. For each structure, the width scaling factor is fixed to $SF_\mathrm{w} = 0.004$ m, the initial cell width to $W_1 = 0.06$ m, the cell height to $H = 0.05$ m, and the number of resonators to $N_\mathrm{r} = 5$. Figure 3(a) shows the comparative transmission coefficient for both the FEM and TMM simulations for the various N_c values. With only a single cell, the first four individual resonance frequencies corresponding to the four longer resonators can clearly be seen with the fifth resonance lying higher than f_h. Due to the small number of total resonators within the single-celled structure, large gaps of increased transmission lie between each resonance and the overall TL is relatively low. Adding an additional 2 cells is shown to significantly decrease these peaks leading to a more complete attenuation of frequencies with smaller overall transmission. With a total of five cells, the muffler achieves comprehensive broadband attenuation from 630 Hz to 1940 Hz with no significant peaks in transmission. This confirms that the interactions among the individual resonators can effectively broaden the bandwidth

of the structure because of the coupling effects. It is therefore important to choose the number of cells such that the desired attenuation is obtained without the addition of unnecessary cells. Under 500 Hz the TMM model tends to show a downward shift in frequency response compared to that of the simulation. Above 500 Hz, the TMM model transitions to an upwards shift which increases at higher frequencies. This variation is a result of simplifications within the TMM model, such as the neglection of evanescent interactions between each resonator and the exclusion of the effects due to bend location within the resonators.

We then vary the width scaling factors SF_w from 0.001 m to 0.003 m to study the effects of resonance frequency overlap between the cells. For each structure, the cell number is fixed to $N_c = 5$, the initial cell width to $W_1 = 0.06$ m, the cell height to $H = 0.05$ m, and the number of resonators per cell to $N_r = 5$. As seen in figure 3(b), there exists a value for the width scaling factor for a specific structure such that transmission peaks are minimized. With $SF_w = 0.001$ m, large gaps in attenuation exist at approximately 850 Hz, 1100 Hz, and 1500 Hz. Increasing the width scaling factor to $SF_w = 0.002$ m significantly decreases these peaks while also slightly shifting them down in frequency. At $SF_w = 0.003$ m, the attenuation gaps have largely been eliminated. This trend indicates that a moderate scaling factor is needed to reduce the undesired overlap in the resonance frequencies from the resonators in each cell. By choosing an optimal value for SF_w, each cell contains resonators of unique lengths, leading to an optimally detuned structure.

Finally, the low frequency performance of the silencer is examined in the context of the starting cell width. For each structure in this study, the cell number is fixed to $N_c = 3$ to minimize axial length of the muffler as to maintain compactness. Width scaling factor is fixed to $SF_w = 0.004$ m, cell height to $H = 0.10$ m, and the number of resonators per cell to $N_r = 5$. Figure 3(c) compares the transmission coefficient for structures with starting cell width $W_1 = 0.10$ m and $W_1 = 0.20$ m. For $W_1 = 0.10$ m, the TMM and FEM simulations show a low frequency limit of 308 Hz. Doubling the starting cell width to $W_1 = 0.20$ m extends this frequency to approximately 173 Hz, with a tradeoff of increasing the frequency gap between each resonator, resulting in the appearance of more transmission peaks within the target frequency band. Increasing W_1 beyond this will further decrease the low frequency limit of the muffler at the cost of axial length. With only $N_c = 3$ cells, it is difficult to achieve broadband sound attenuation, as some high transmission is observed at certain frequencies. This can be improved by adding additional cells, though practical space constraints may dictate the viability of this since each additional cell is accompanied by a large increase in axial length.

Additionally, it is noted that a larger variation in predictions exists between the FEM and TMM models above 500 Hz. The primary cause of this variation is the simplification of the effects of bending the resonators. Holding H constant, an increase in cell width results in a bend location farther from the midpoint of each resonator. Since the analytical model assumes a bend location of $0.5R_{cav}$, as values for W_1/H increase considerably past 1, the model tends to show decreased agreement with FEM simulations.

While not studied here, another way to achieve low frequency attenuation is to increase cell height H. Keeping W_1 constant, a larger cell height will similarly result in a decrease in the lower frequency limit for the silencer by increasing the volume of the resonators.

3.2. Optimized structure

As discussed above, the geometric parameters of the silencer play an important role in determining the acoustic performance of the silencer. Since these parameters are interdependent on one another within a fixed overall dimension (where a larger volume will generally enhance acoustic performance), a systematic optimization process is needed to find the optimal configuration of the silencer under given design constraints. To achieve this, we first define loose bounds for some of the geometric properties discussed in section 2.1. This helps to ensure sufficient flexibility for optimization while adhering to dimensional constraints. A customized algorithm then computes the sound transmission characteristics using the TMM model and iteratively solves for the optimal geometry. In each iteration, the transmission coefficient is summed within the target frequency range and recorded as a score for that geometry. Each frequency within the target range is assigned an equal weight using a flat incident SPL spectrum. The objective function for optimization is described as:

$$\min O(x) = \sum_{f=f_{\min}}^{f_{\max}} \tau_f(x) \tag{17}$$

where the frequency is increased linearly in steps of 1 Hz from $f_{\min}$ to $f_{\max}$ Here, x denotes the full set of design parameters defining the silencer geometry. The structure with the lowest score is then returned

Table 2. Geometric properties of optimized muffler.

Property	R_d (m)	W_1 (m)	H (m)	SF_w (m)	N_c	N_r	d_t (m)	L_{cav} (m)
Value	0.050	0.057	0.050	0.004	5	5	0.002	0.0076

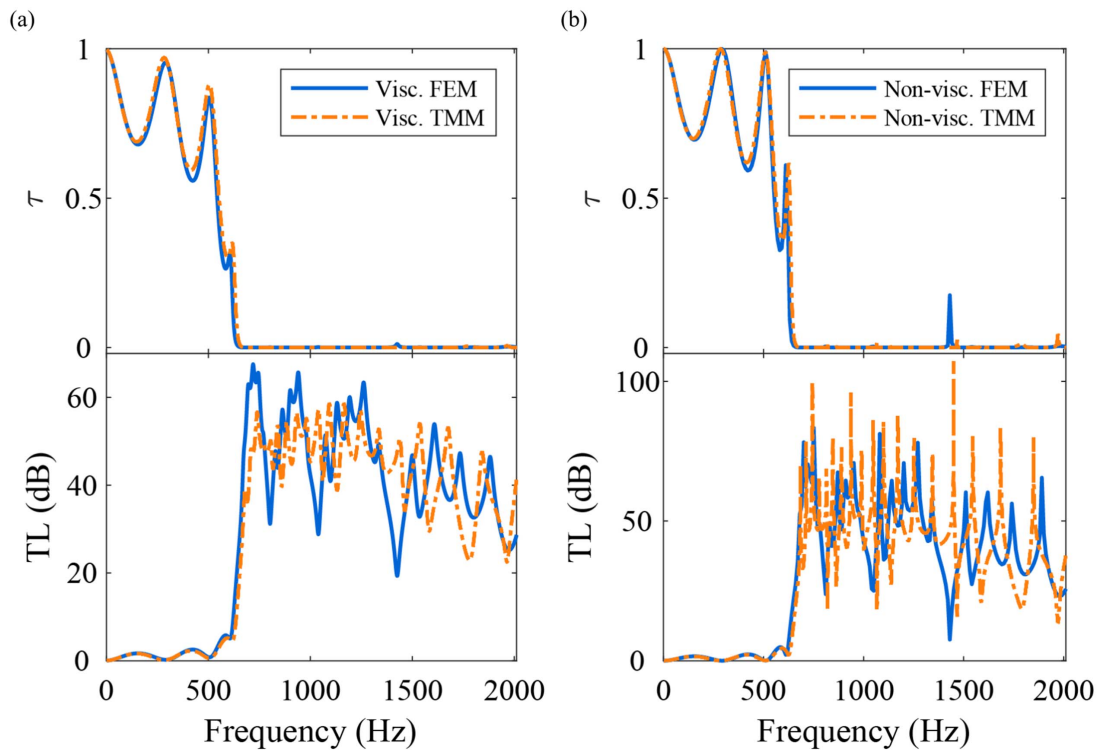

Figure 4. Comparative transmission of optimized structure between FEM simulations and TMM model. Transmission and TL curves by (a) including viscothermal losses and (b) neglecting viscothermal losses.

and presented as the optimized geometry. This approach adds great flexibility to the design of the silencer, as the frequency range can be freely selected for specific applications. Different weights of the frequencies can also be included in the algorithm so that multi-band sound attenuation can be achieved. Moreover, our approach has the ability to add a penalty to the score depending on the total physical volume of the structure, so that the optimization balances between performance and footprint.

An optimized muffler is now presented using the approach described above. Cell height is fixed to $H = 0.05$ m to maintain radial compactness, wall thickness is fixed to $d_t = 0.002$ m, and the target frequency range is set from 650 Hz to 2000 Hz. Running the parametric optimization script with moderate bounds on the remaining geometric properties, the final optimized muffler is calculated and presented in table 2. The total external length and diameter of the structure are 0.325 m and 0.200 m, respectively, with a total volume usage outside the main duct of 0.007 66 m^3.

Figure 4(a) displays the final transmission coefficient τ and the TL for the FEM and TMM simulations including viscothermal interactions. For both models, τ is below 0.01 from 653 Hz up to f_h, demonstrating excellent sound attenuation properties. The transmission behavior is well explained by both models, with the TMM showing a slight underestimation of TL near the low-frequency limit of the device. Figure 4(b) displays the transmission coefficient τ and the TL for the FEM and TMM simulations without viscothermal interactions. It is shown that, while many sharp peaks in TL are present due to the absence of viscothermal damping, these interactions do not play a major role in the acoustic performance of the proposed structure. This agrees with the results discussed previously in [25], and suggests that the silencer does not rely on fine tuning of the viscothermal effects.

While the frequency band chosen for the optimized structure achieves a tuning ratio of $f_2/f_1 \approx 3$, the core methodology of the structure's tunable design allows for accurate adjustments to target many other frequency ranges. Moreover, the optimized band has practical use cases in many applications. Tonal noise generated by combustion engines is typically most prominent from 800 Hz to 4000 Hz as this range represents the band with least structural attenuation [53]. Additionally, various HVAC components generate tonal noise in discrete bands over which the proposed silencer could be easily adapted

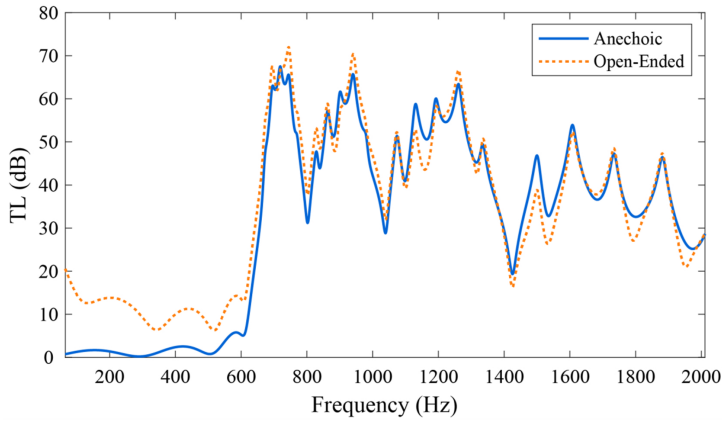

Figure 5. Comparison of optimized structure's TL with an anechoic termination and an open-ended termination.

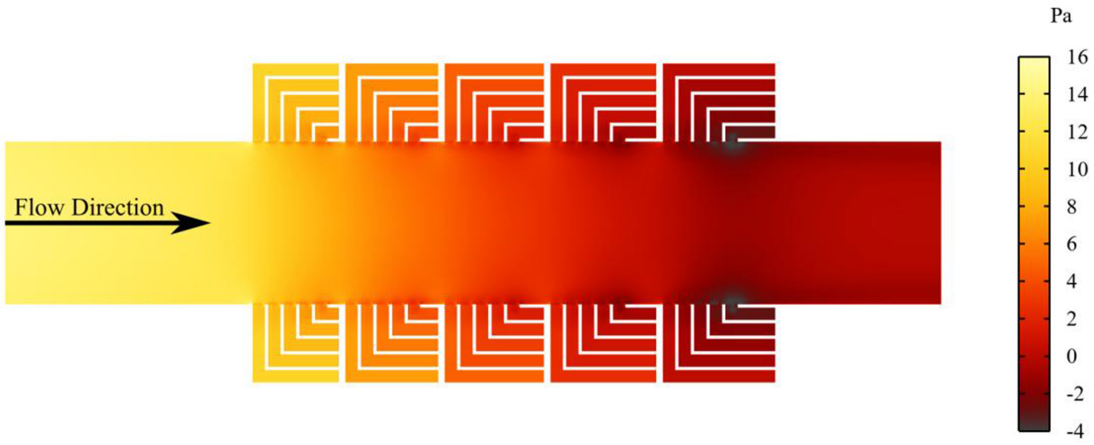

Figure 6. Surface plot of fluid static pressure drop across the optimized structure.

for with minor tuning variations [54]. Though the target frequency range chosen for optimization was selected for the sake of experimental convenience, attenuation of much lower frequencies can also be readily achieved using the same design methodology by updating the configuration of the silencer.

The performance of the silencer with an anechoic termination is now compared with its performance when the outlet is exposed to the environment in an open-ended scenario. To accomplish this, the FEM simulation is modified to incorporate an impedance boundary condition at the outlet. The boundary is configured to represent the impedance of an open-ended, unflanged circular pipe with the duct radius defined accordingly. The results seen in figure 5 show that the silencer is minimally affected by an open-ended termination, with a slight increase in TL under the low-frequency limit of the device. Above this limit, no major variation in transmission is exhibited by the silencer. These results demonstrate the strong inherent acoustic performance of the device and prove its suitability for realistic open-ended configurations such as those found in automotive exhaust systems.

To confirm the ventilation performance of the proposed silencer, pressure drop due to grazing flow is simulated using COMSOL Multiphysics with the turbulent flow, k–ω physics model. Using 2D-axisymmetric geometry, the inlet is set to a fully developed flow boundary condition at 10.29 m s^{-1}, and the outlet is defined as a pressure outlet boundary condition. Flow is modeled as compressible, and walls are treated with a roughness of 5 μm. As shown in figure 6, the final static pressure drop across the structure is calculated to be 14.5 Pa which is in line with other similar metamaterial structures [33]. These results demonstrate a very low fluid pressure drop, indicating that the silencer introduces only minimal flow resistance. Such low flow resistance ensures the silencer can maintain acoustic control without significantly restricting ventilation.

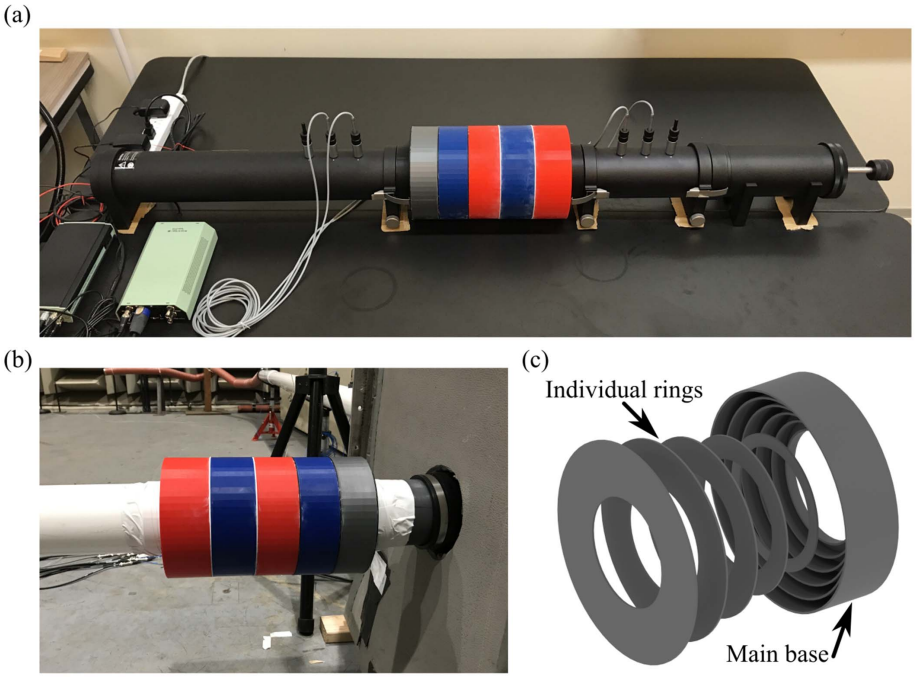

Figure 7. (a) Experimental setup for transmission tube measurements. (b) Experimental setup for transmission loss measurements with grazing flow. (c) Exploded view of 3D printing split for a single cell.

4. Experimental results

In this section, the calculated TL of the optimized muffler is compared against the results obtained from experimental measurement. The stationary experimental results were obtained using a Brüel & Kjær (B&K) Transmission Tube Type 4206-T with B&K Type 4187 microphone capsules. The loudspeaker was driven by a 5 s linear frequency sweep from 20–22 000 Hz. Following ASTM 2611 measurement procedure, four microphones were flush mounted inside the transmission tube, with two sets positioned on both sides of the muffler. The experimental setup with the muffler mounted on the transmission tube is shown in figure 7(a).

The muffler's acoustic performance under grazing flow was also experimentally measured by connecting the structure downstream of a large industrial blower in an anechoic chamber as shown in figure 7(b). The blower was set to a volumetric flow rate of 270 $\pm$ 5 cfm, resulting in a flow velocity of approximately 16 m s^{-1}. Readings were taken in the tube downstream of the muffler. The muffler was then removed from the system and readings were again taken to form the baseline data. The TL of the muffler under grazing flow was obtained by performing a difference operation between the baseline and attenuated data.

The muffler was fabricated using fused deposition modeling 3D printing with high-strength polylactic acid (PLA) filament on a heated bed to reduce warping. It is noted that while PLA allows for rapid fabrication and testing, other materials such as thermoplastic polyurethane can be used for improved durability and mechanical strength. Due to the complex space-folded geometry of the structure, each cell was divided into 5 individual disks along with a main base which were then glued together as shown in figure 7(c). This was done to mitigate the need for support structures, leading to a higher quality surface finish and greater dimensional accuracy. Each part was printed with solid infill to increase strength and ensure structural consistency.

Under stationary conditions, the muffler achieved an average experimental TL of 36.3 dB within the target frequency range of 650–2000 Hz, with a minimum TL of 19.7 dB. A comparison between TMM, FEM and experimental transmission coefficient is shown in figure 8(a). It is observed that both models show great agreement with the experimental results. Additionally, the muffler exhibits a pronounced attenuation over a subset of frequencies between 900 Hz and 1250 Hz, which marginally declines from 1250 Hz to f_h. An average TL of 42.8 dB is calculated over this subset, indicating exceptionally high reactivity across this frequency band. Compared to standard straight-through perforated tube silencers, this device achieves much more uniform and complete attenuation [55, 56]. Additionally, this device can be precisely tuned to any desired frequency range without the need for complex micro-perforated panels.

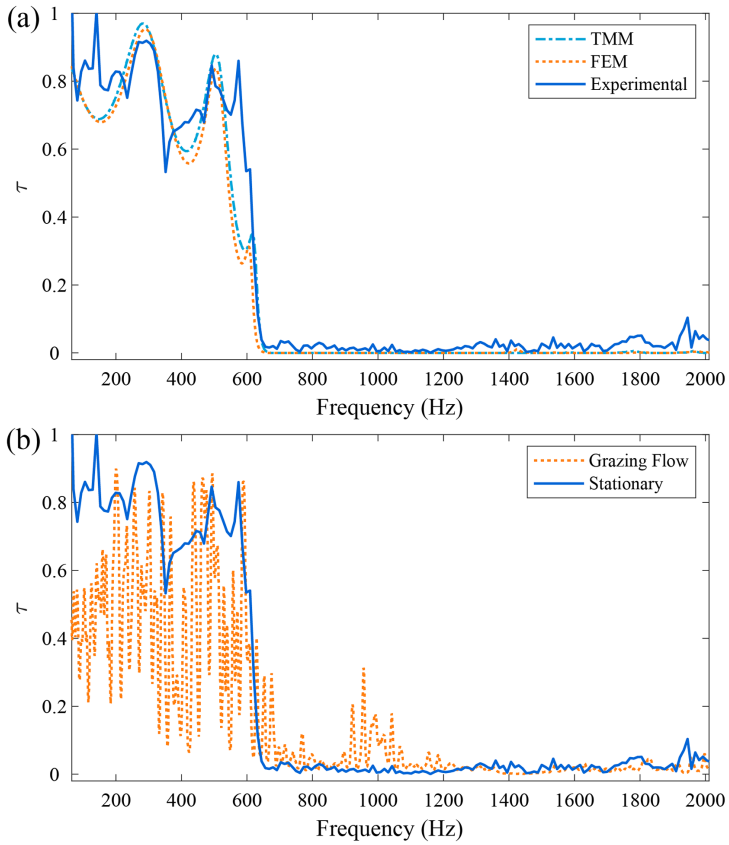

Figure 8. Experimental results. (a) Comparative transmission coefficient of optimized structure between TMM, FEM and experimental measurements for the stationary condition. (b) Transmission coefficient of the optimized structure in grazing flow and stationary conditions.

The grazing flow transmission data is seen in figure 8(b) along with the stationary condition transmission for reference. Compared to the case of no background flow, a decreased performance is observed, and the average TL drops to 17.2 dB across the target frequency range. The data also tends to contain significantly more noise compared to the stationary results below the cutoff frequency. On the other hand, the lower frequency limit is still accurately captured by the experimental results and agrees well with the calculations. Above that frequency, consistent low transmission coefficient is observed. Several factors could contribute to the reduced attenuation and discrepancies observed in the measurement data under grazing flow conditions. First, the blower generates a loud noise outside the tube which is difficult to be totally concealed from the measurement position. Second, the connection points between the silencer and the tube may not be perfectly sealed as those in the transmission tube setup. Third, due to the nature of the PLA material used to construct the device, a slight flexibility is observed in the internal disks, possibly leading to a deformation of the structure under moderate flow. Finally, the airflow in the duct may generate strong noise by interacting with the structure through flow acoustic coupling [57, 58]. To confirm this, a multiphysics simulation that is carried out in COMSOL by combining the turbulent flow and the acoustic waves via the aeroacoustic flow source coupling. Consistent with the measurements, an incoming flow with velocity of 10.29 m s^{-1} is modeled at the upstream of the silencer, and the corresponding turbulent flow and flow-induced noise are analyzed. Thanks to the small slit width and no obstruction to the main duct, the flow field maintains relatively uniform in the duct, as shown in figure 9(a). On the other hand, the flow-induced noise extracted at the downstream of the silencer exhibits a high SPL, especially at low and mid-frequency ranges. From figure 9(b), the average SPL generated by the flow is around 40 dB under 2500 Hz and can reach above 60 dB at certain frequencies. The results indicate that the flow-induced noise may be contributing to the variations in the measurement below 600 Hz, as the designed silencer does not insulate sound well at these frequencies.

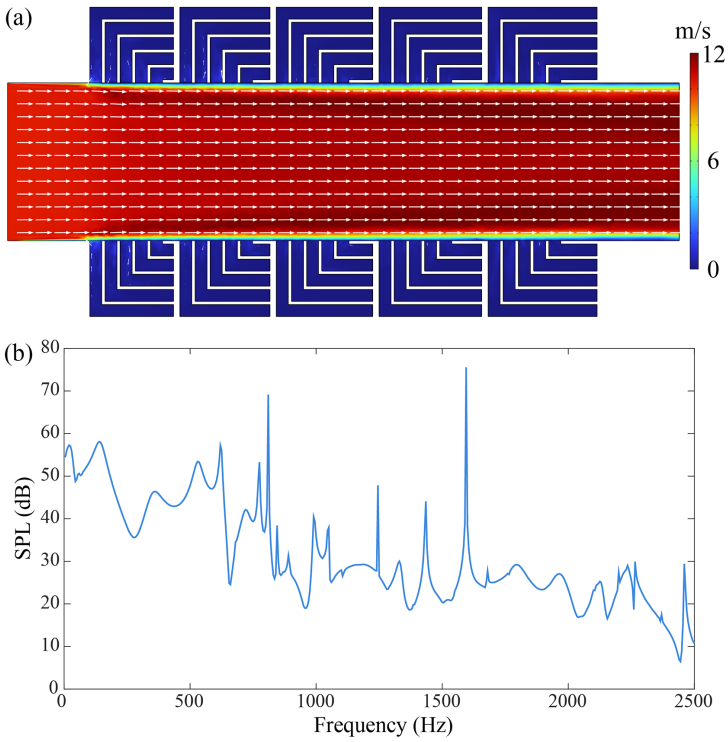

Figure 9. Flow-acoustic interaction of the silencer in a duct with airflow. (a) Velocity distribution of the flow field. The white arrows denote the direction of the airflow. (b) SPL of flow-induced noise in the duct.

5. Conclusion

A compact reactive silencer containing space-folded concentric resonators capable of broadband frequency attenuation has been proposed. An analytical TMM model is presented and validated using COMSOL Multiphysics through a set of parametric studies. The analytical model accounts for visco-thermal losses as well as the effect of folding the resonators using a simplified effective length. It is shown in the parametric studies that the linking of additional cells to the structure leads to a more complete attenuation within the target frequency range while compromising axial compactness. It is found that, for a specific structure configuration, a width scaling factor exists that minimizes transmission for that structure. It is therefore necessary to choose the correct geometric properties as to attain the desired acoustic performance without unnecessary size increase. The low-frequency capabilities of the design are also recognized by increasing starting cell width, thus increasing the overall resonator lengths.

Using a customized optimization approach, a silencer is designed to operate from 650 Hz to 2000 Hz while being constrained to a maximum diameter of 0.200 m. With a total volume usage outside the main duct of 0.007 66 m^3, the optimized structure exhibites significant attenuation across the target frequency range, as confirmed by both TMM and FEM results. Using turbulent flow simulations in COMSOL, the structure displays good aerodynamic performance with a pressure drop of only 14.5 Pa due to the open-channel design. The optimized muffler is also tested experimentally in both stationary and grazing flow. In stationary flow, the optimized muffler achieves an average TL of 36.3 dB over the target frequency range, dropping to 17.2 dB in grazing flow at a volumetric flow rate of 270 $\pm$ 5 cfm. These results demonstrate the practical utilization of the silencer under different conditions.

The proposed device shows promise for real-world applications requiring pre-defined attenuation without inhibiting fluid flow through a duct. The ability to tune the structure's primary frequency band while considering size constraints allows for customization to meet specific application needs. By parametrically optimizing the geometry, the design achieves a compact size while maintaining effective noise reduction and minimal pressure drop, demonstrating applicability in many industrial and commercial systems. The theoretical and numerical models can be integrated into other optimization techniques including inverse design approaches [59] for other applications with user-desired performance.

Finally, it is important to note some avenues for future improvement for this device. First, although high strength PLA filament is used to provide a convenient means for fabrication with acceptable mechanical stability during testing, stronger materials will likely be needed should high flow rate be

implemented. Second, although the effective length to account for the bending of the resonators helps to bring the TMM into closer agreement with FEM simulations, it is unable to accurately predict the characteristics of the structure with excessive W_1/H values. A more thorough investigation of the bending characteristics of such a device is of particular significance for the future development of the structure, which will enable more complex geometries and a wider combination of unit cell architectures.

Data availability statement

The data cannot be made publicly available upon publication because they are not available in a format that is sufficiently accessible or reusable by other researchers. The data that support the findings of this study are available upon reasonable request from the authors.

Acknowledgments

The authors would like to thank Gower Choi and Tommy Tang for their help with the measurement and valuable contributions to this work. The use of anechoic chamber at the Naval Surface Warfare Center Philadelphia Division is gratefully acknowledged. This work was supported by the National Science Foundation under Grant Nos. CMMI-2137749 and ECCS-2337069.

Conflict of interest

The authors declare that they have no known competing financial interests or personal relationships that could have appeared to influence the work reported in this paper.

Author contributions

Joshua Lloyd 0009-0008-8251-3796
Conceptualization (equal), Data curation (equal), Investigation (equal), Methodology (equal), Software (equal), Writing – original draft (equal), Writing – review & editing (equal)

Chadi Ellouzi 0009-0009-7185-754X
Investigation (equal), Writing – review & editing (equal)

Farhood Aghdasi
Investigation (equal), Writing – review & editing (equal)

Chen Shen 0000-0003-3535-8494
Conceptualization (equal), Funding acquisition (equal), Investigation (equal), Methodology (equal), Supervision (equal), Writing – review & editing (equal)

References

[1] Mei J, Ma G, Yang M, Yang Z, Wen W and Sheng P 2012 Dark acoustic metamaterials as super absorbers for low-frequency sound *Nat. Commun.* **3** 758
[2] Sagartzazu X, Hervella-Nieto L and Pagalday J M 2008 Review in sound absorbing materials *Arch. Comput. Methods Eng.* **15** 311–42
[3] Yang M and Sheng P 2024 Sound absorption structures: from porous media to acoustic metamaterials keynote topic *Annu. Rev. Mater. Res.* **10** 41
[4] Jafari M J, Monazam M R and Kazempour M 2018 Providing an optimal porous absorbent pattern to reduce mid to low-frequency sounds *J. Environ. Health Sci. Eng.* **16** 289–97
[5] Ren S, Liu Y, Sun W, Wang H, Lei Y, Wang H and Zeng X 2022 Broadband low-frequency sound absorbing metastructures composed of impedance matching coiled-up cavity and porous materials *Appl. Acoust.* **200** 109061
[6] Yang J, Lee J S and Kim Y Y 2015 Metaporous layer to overcome the thickness constraint for broadband sound absorption *J. Appl. Phys.* **117** 174903
[7] Xiang L, Wang G, Luo G, Shen J, Deng Z and Wen S 2024 Optimization of hybrid microperforated panel and nonuniform space-coiling channels for broadband low-frequency acoustic absorption *Appl. Acoust.* **216** 109763
[8] Yuan T, Song X, Xu J, Pan B, Sui D, Xiao H and Zhou J 2022 Tunable acoustic composite metasurface based porous material for broadband sound absorption *Compos. Struct.* **298** 116014
[9] Cheng B Z, Gao N, Zhang R H and Hou H 2021 Design and experimental investigation of broadband quasi-perfect composite loaded sound absorber at low frequencies *Appl. Acoust.* **178** 108026
[10] Mi Y, Cheng L, Zhai W and Yu X 2022 Broadband low-frequency sound attenuation in duct with embedded periodic sonic black holes *J. Sound Vib.* **536** 117138
[11] Bezançon G, Doutres O, Umnova O, Leclaire P and Dupont T 2024 Thin metamaterial using acoustic black hole profiles for broadband sound absorption *Appl. Acoust.* **216** 109744

[12] Bravo T and Maury C 2023 Broadband sound attenuation and absorption by duct silencers based on the acoustic black hole effect: simulations and experiments *J. Sound Vib.* **561** 117825
[13] Munjal M L 2014 *Acoustics of Ducts and Mufflers* 2nd edn (Wiley)
[14] Tang S K 2010 On sound transmission loss across a Helmholtz resonator in a low Mach number flow duct *J. Acoust. Soc. Am.* **127** 3519–25
[15] Howard C Q and Craig R A 2014 Noise reduction using a quarter wave tube with different orifice geometries *Appl. Acoust.* **76** 180–6
[16] Mercier J-F, Marigo J-J and Maurel A 2017 Influence of the neck shape for Helmholtz resonators *J. Acoust. Soc. Am.* **142** 3703–14
[17] Field C D and Fricke F R 1998 Theory and applications of quarter-wave resonators: a prelude to their use for attenuating noise entering buildings through ventilation openings *Appl. Acoust.* **53** 117–32
[18] Liu J W, Yu D L, Yang H B, Shen H J and Wen J H 2020 Effect of mean flow on acoustic wave propagation in a duct with a periodic array of Helmholtz resonators *Chin. Phys. Lett.* **37** 034301
[19] Bricault C, Meng Y and Goudé S 2022 Optimization of a silencer design using an Helmholtz resonators array in grazing incident waves for broadband noise reduction *Appl. Acoust.* **201** 109090
[20] Cai C and Mak C M 2018 Hybrid noise control in a duct using a periodic dual Helmholtz resonator array *Appl. Acoust.* **134** 119–24
[21] Wang X and Mak C-M 2012 Wave propagation in a duct with a periodic Helmholtz resonators array *J. Acoust. Soc. Am.* **131** 1172–82
[22] Griffin S, Lane S A and Huybrechts S 2001 Coupled Helmholtz resonators for acoustic attenuation *J. Vib. Acoust.* **123** 11–17
[23] Wang X, Zhu W and Zhou Y 2016 Sound transmission in a duct with a side-branch tube array mounted periodically *J. Acoust. Soc. Am.* **139** EL202–8
[24] Nguyen H, Wu Q, Xu X, Chen H, Tracy S and Huang G 2020 Broadband acoustic silencer with ventilation based on slit-type Helmholtz resonators *Appl. Phys. Lett.* **117** 134103
[25] Červenka M, Bednařík M and Groby J-P 2019 Optimized reactive silencers composed of closely-spaced elongated side-branch resonators *J. Acoust. Soc. Am.* **145** 2210–20
[26] Červenka M and Bednařík M 2020 Optimized compact wideband reactive silencers with annular resonators *J. Sound Vib.* **484** 115497
[27] Ang L Y L, Cui F, Lim K M and Lee H P 2023 A systematic review of emerging ventilated acoustic metamaterials for noise control *Sustainability* **15** 4113
[28] Gao N, Zhang Z, Deng J, Guo X, Cheng B and Hou H 2022 Acoustic metamaterials for noise reduction: a review *Adv. Mater. Technol.* **7** 2100698
[29] Dong R, Sun M, Mo F, Mao D, Wang X and Li Y 2021 Recent advances in acoustic ventilation barriers *J. Appl. Phys.* **54** 403002
[30] Kheybari M and Ebrahimi-Nejad S 2019 Locally resonant stop band acoustic metamaterial muffler with tuned resonance frequency range *Mater. Res. Express* **6** 025802
[31] Kheybari M and Ebrahimi-Nejad S 2021 Dual-target-frequency-range stop-band acoustic metamaterial muffler: acoustic and CFD approach *Eng. Res. Express* **3** 035027
[32] Su Z, Zhu Y, Gao S, Luo H and Zhang H 2022 High-efficient and broadband acoustic insulation in a ventilated channel with acoustic metamaterials *Front. Mech. Eng.* **8** 857788
[33] Zhang D, Su X, Sun Y, Luo Y, Sun X and Chen C 2024 Performance study and improvement of space-folded metamaterial muffler for pipe under grazing flow *Appl. Acoust.* **220** 109984
[34] Kim D Y, Ih J G and Åbom M 2020 Virtual Herschel-Quincke tube using the multiple small resonators and acoustic metamaterials *J. Sound Vib.* **466** 115045
[35] Xu Z X, Qiu W J, Cheng Z Q, Yang J, Liang B and Cheng J C 2024 Broadband ventilated sound insulation based on acoustic consecutive multiple Fano resonances *Phys. Rev. Appl.* **21** 044049
[36] Ghaffarivardavagh R, Nikolajczyk J, Anderson S and Zhang X 2019 Ultra-open acoustic metamaterial silencer based on Fano-like interference *Phys. Rev. B* **99** 024302
[37] Liu Y, Zhang W, Cao G, Zuo G, Liu C and Ma F 2024 Ultra-thin ventilated metasurface pipeline coating for broadband noise reduction *Thin-Walled Struct.* **200** 111916
[38] Guan Y J *et al* 2024 An ultra-low-frequency sound absorber and its application in noise reduction in ducts *APL Mater.* **12** 011127
[39] Wang X, Xu S, Bai Y, Luo X, Yang M and Huang Z 2024 Meta-barriers for ventilated sound reduction via transformation acoustics *Int. J. Mech. Sci.* **274** 109262
[40] Zhu Y, Dong R, Mao D, Wang X and Li Y 2023 Nonlocal ventilating metasurfaces *Phys. Rev. Appl.* **19** 014067
[41] Xu Z X, Gao H, Ding Y J, Yang J, Liang B and Cheng J C 2020 Topology-optimized omnidirectional broadband acoustic ventilation barrier *Phys. Rev. Appl.* **14** 054016
[42] Liu C *et al* 2021 Three-dimensional soundproof acoustic metacage *Phys. Rev. Lett.* **127** 084301
[43] Wu X *et al* 2018 High-efficiency ventilated metamaterial absorber at low frequency *Appl. Phys. Lett.* **112** 103505
[44] Li X, Zhang H, Tian H, Huang Y and Wang L 2022 Frequency-tunable sound insulation via a reconfigurable and ventilated acoustic metamaterial *J. Appl. Phys.* **55** 495108
[45] Wen G, Zhang S, Wang H, Wang Z-P, He J, Chen Z, Liu J and Xie Y M 2023 Origami-based acoustic metamaterial for tunable and broadband sound attenuation *Int. J. Mech. Sci.* **239** 107872
[46] Jin X, Fang H, Yu X, Xu J and Cheng L 2023 Reconfigurable origami-inspired window for tunable noise reduction and air ventilation *Build. Environ.* **227** 109802
[47] Ravanbod M, Ebrahimi-Nejad S and Mollajafari M 2024 A thin-walled cavity structure with double-layer tapered scatterer locally resonant metamaterial plates for extreme low-frequency attenuation *Int. J. Solids Struct.* **293** 112742
[48] Shen C, Xie Y, Li J, Cummer S A and Jing Y 2018 Acoustic metacages for sound shielding with steady air flow *J. Appl. Phys.* **123** 124501
[49] Cambonie T, Mbailassem F and Gourdon E 2018 Bending a quarter wavelength resonator : curvature effects on sound absorption properties *Appl. Acoust.* **131** 87–102
[50] Dell A, Krynkin A and Horoshenkov K V 2021 The use of the transfer matrix method to predict the effective fluid properties of acoustical systems *Appl. Acoust.* **182** 108259
[51] Zwikker C and Kosten C W 1949 *Sound Absorbing Materials* (Elsevier Publishing Company, Inc)
[52] Stinson M R 1991 The propagation of plane sound waves in narrow and wide circular tubes, and generalization to uniform tubes of arbitrary cross- sectional shape *J. Acoust. Soc. Am.* **89** 550–8
[53] Sheng G 2012 *Vehicle Noise, Vibration, and Sound Quality* (SAE International)

[54] Bujoreanu C and Benchea M 2016 Experimental study on HVAC sound parameters *IOP Conf. Ser.: Mater. Sci. Eng.* **147** 012051
[55] Demír A and Büyükaksoy A 2005 Wiener-Hopf approach for predicting the transmission loss of a circular silencer with a locally reacting lining *Int. J. Eng. Sci.* **43** 398–416
[56] Alisah M I, Ooi L-E, Ripin Z M, Yahaya A F and Ho K 2021 Acoustic attenuation performance analysis and optimisation of expansion chamber coupled micro-perforated cylindrical panel using response surface method *Arch. Acoust.* **46** 507–17
[57] Lafon P, Caillaud S, Devos J P and Lambert C 2003 Aeroacoustical coupling in a ducted shallow cavity and fluid/structure effects on a steam line *J. Fluids Struct.* **18** 695–713
[58] Zhang S, Song A, Wang S and Yu X 2025 Broadband sound insulation of an open duct with side-branch resonators in airflow environment *Results Phys.* **75** 108324
[59] Dong H W *et al* 2024 Inverse design of phononic meta-structured materials *Mater.Today* **80** 824–55